Journal of Thermal Stresses, 37: 870–883, 2014

ISSN: 0149-5739 print/1521-074X online
DOI: 10.1080/01495739.2014.912919

Taylor & Francis
Taylor & Francis Group

FINITE ELEMENT ANALYSIS OF THERMOELASTIC INSTABILITY IN INTERMITTENT SLIDING CONTACT

Yun-Bo Yi[1], Ali Bendawi[1], Heyan Li[2], and Jiaxin Zhao[2]
[1]*Department of Mechanical and Materials Engineering, University of Denver, Denver, Colorado, USA*
[2]*School of Mechanical Engineering, Beijing Institute of Technology, Beijing, P.R. China*

A finite element model is developed for the frictionally excited thermoelastic instability problem in intermittent sliding contact with finite geometries and realistic friction materials. The existing analytical solutions are used to validate the method in several limiting cases. It is concluded that some caution must be taken for the commonly used strategy of assuming time-averaged frictional heat generation for intermittent contact. The predictions made by the half-plane analytical solution that assumes thermally nonconductive and rigid frictional surface considerably overestimate the dimensionless critical speeds of realistic brake or clutch systems. Longer wavelength perturbations become unstable at a dimensionless sliding speed approaching zero, as opposed to the converged value of unity in the half-plane solution. Averaging the heat input over the entire circumference is appropriate only when the period of frictional contact is longer than that of separation. These results merit the use of the finite element method in more general applications involving intermittent contact.

Keywords: Brake; Clutch; Finite element; Intermittent contact; Thermoelastic instability

INTRODUCTION

Thermoelastic instability (TEI) theory states that in frictional sliding systems such as disk brakes or clutches, the thermal-mechanical feedback can be unstable if the sliding speed exceeds a certain threshold [1]. The theoretical models were developed over the past decades to investigate the phenomenon, both analytically [2] and numerically [3], using either the eigenvalue formulation [4] or transient simulation [5], the former of which assume a perturbation of the solution in the exponentially growing form, and an eigenvalue equation is constructed from the governing differential equations. The growth rates of the variables, and further the critical sliding velocity, can then be recovered from the eigenvalues of the equation.

The majority of these works assume coextensive contact, especially for clutch systems, due to the fact that they have annular geometries, moving continuously

Received 15 August 2013; accepted 10 October 2013.
Address correspondence to Yun-Bo Yi, Department of Mechanical and Materials Engineering, University of Denver, Denver, Colorado 80208, USA. E-mail: yun-bo.yi@du.edu
Color versions of one or more of the figures in the article can be found online at www.tandfonline.com/uths.

in the circumferential direction. Many other sliding surfaces, such as those in disk brake systems, are not coextensive as the brake pads do not cover the entire rotor surface, and the material points on a surface always experience alternating periods of contact and separation. For axisymmetric plates in clutches, intermittent processes are also possible, e.g., in the presence of initially uneven surfaces as a result of surface separation, manufacturing imperfection, or misalignment of the axles during mounting.

These intermittent processes can be expected to alter the stability boundaries of the TEI problem. Barber et al. [6] suggested us to allow for the intermittent contact in TEI by averaging the heat input over the circumference. This strategy was later reiterated by some other researchers, such as Hartsock and Fash [7]. However, the hypothesis was not verified until Ayala et al. [8], who explored a simplified intermittent contact problem in which an infinite, conductive material slides against a rigid nonconductive surface. Their results show that at a low Fourier number, i.e. when the thermal transient is much longer than the period of one revolution, the method by averaging the frictional heat input over the circumference works fairly well, and the critical speed is an inverse linear function of the proportion of time in sliding contact. However, at higher Fourier numbers the critical speed becomes lower, although the dependence of the critical speed on the Fourier number becomes relatively weak.

These conclusions, however, were based on the assumption that the friction material is rigid and nonconductive, and that the other material has an infinite extension. Realistic geometries do not satisfy these idealized conditions. Prior researches on continuous contact revealed considerable differences between the half-plane solutions and the models with finite dimensions and real materials [9, 10]. It is not clear at this point whether the same conclusions obtained from the idealized half-plane solutions equally work for more realistic systems involving finite geometries with both materials being deformable and conductive.

The analytical approaches have proved difficult in handling this type of problems due to the demand for numerical convergence and iterations, which are sometimes computationally prohibitive. The finite element method developed by Yi et al. [11] is therefore a preferable tool, and the present work is devoted to solving the intermittent contact problem using the same strategy. It should be pointed out that some preliminary discussions on this issue can be found in the literature [12]; however, a systematic exploration of the problem including the method validation has never been attempted.

FINITE ELEMENT MODELS

General Formulation

We assume a two-dimensional configuration to approximate a brake or clutch. The circumference of a brake or clutch disk is spread out along the sliding direction, and the effect of the radial thickness is ignored in our model. The solution method follows the standard procedure for the problems in this category [11]. Briefly one can start from the governing equations of heat conduction, thermoelasticity and frictional heat generation. It is followed by a search for the constant speed solution

in linear perturbations that grow exponentially in time. For the temperature field, the perturbation solution can be written as

$$T(x, y, t) = T_0(x, y) + \Re\{e^{bt} T_1(x, y)\} \tag{1}$$

where T_0 is the steady-state solution, b is a complex exponential growth rate. $\Re$ represents the real part of a complex number. The amplitude of oscillation T_1 is typically complex to reflect the change in the phase angle of temperature across the thickness. Similar assumptions in the perturbation form can be made on other key variables including the displacement and the contact pressure. A direct result from the perturbation assumption is that time is eliminated from the governing equations, leading to a generalized eigenvalue equation in the following matrix form after an implementation of the finite element method:

$$\mathrm{M}\Theta = b\mathrm{H}\Theta \tag{2}$$

where Θ is the nodal temperature vector; M and H are the coefficient matrices determined from the material properties and the finite element shape functions.

Given appropriate boundary conditions the critical speed can be determined from the sliding speed at which the real part of the growth rate is zero. Notice that in the above formulation, the wave number (i.e., the number of higher temperature regions in the sliding direction) is not a predefined parameter. Rather, it is a result obtained from the computed eigenfunctions. Therefore the method can be used to solve problems for both continuous and intermittent contacts. The details on the matrix derivations are omitted here, as they are modified versions of those used in the finite element scheme previously developed by the Yi et al. [11]. In intermittent contact the critical speed is presented as a function of the Fourier number, which is defined by

$$F_o = km^2 t_0 \tag{3}$$

where

$$m = \frac{n}{r}, \quad t_0 = \frac{L}{V} \tag{4}$$

Here, n is the total number of waves in the circumference; r is the radius of the rotating disk, L is the circumferential length; V is the sliding velocity.

Two-Dimensional (2-D) Finite Element Model

In the 2-D finite element model, the mesh is generated uniformly in the sliding direction, but biased towards the contact surfaces in both materials. The implementation of the quadratic element type more accurately approximates the nonlinear distributions of temperature in both thickness and longitudinal directions, and it can thus improve the numerical efficiency. The total length of the model in the y-direction is set to the circumferential length of the disk. In a continuous contact situation, both layers in contact are coextensive with the same length, whereas in an intermittent contact the friction layer has a reduced length (see Figure 1).

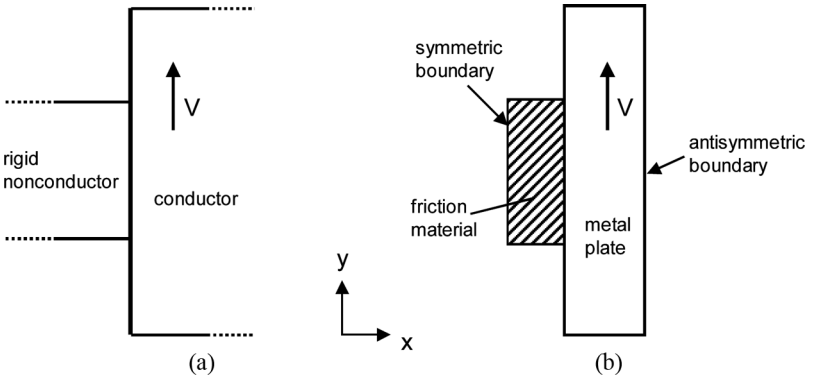

Figure 1 Schematic of the intermittent contact model: (a) a conductive half plane sliding against a rigid nonconductor, and (b) a conductive plate of finite thickness sliding against a deformable and conductive surface.

The frame of reference is fixed to the friction layer to ensure that the problem has a fixed boundary as opposed to a moving one, which is mathematically more difficult to handle. A cyclic boundary condition, i.e., all the quantities on one end are assumed to be the same as those on the other end, is applied to the conductive layer in the direction of sliding to model the closed disk ring configuration. Notice that there are no constraints applied on the ends of the friction pad in the direction of sliding. To simplify the model, the symmetric-antisymmetric boundary conditions are assumed across the thickness (see Figure 1), with the symmetric condition specified on the poor conductor (i.e., the friction material) and the antisymmetric condition on the good conductor (i.e., the metal plate), due to the fact that this mode pattern has been found dominant in many practical applications. Particularly, on the symmetric boundary

$$q_x = 0; \quad u_x = 0; \quad \sigma_{xy} = 0 \tag{5}$$

and on the antisymmetric boundary,

$$T = 0; \quad u_y = 0; \quad \sigma_{xx} = 0 \tag{6}$$

where u, q, and σ represent the displacement, heat flux and stress, respectively. It should be reiterated that the wave number is not predesignated in the two-dimensional model, nor a monotonic function of the sliding speed. Therefore iterations are required to determine the critical speeds and the associated wave numbers. More specifically the critical speed is sought on the basis of the following procedure:

1. The analysis is performed at a number of different sliding speeds with a prescribed interval, and the growth rates of temperature at each sliding speed are computed.
2. The wave number associated with each growth rate b is determined by the Fast Fourier Transform (FFT) technique. This is not a trivial part of the work since

the sinusoidal profiles of the eigenfunctions in continuous contact become highly distorted when intermittent contact is involved.

3. The growth rates of temperature for each wave number at the different sliding speeds are sorted following the above two steps. Three successive sliding speeds with positive growth rates are then identified.
4. The value of the sliding speed at zero growth rate, i.e., the critical speed for each wave number, is extrapolated by quadratic curve fitting on the basis of the three different pairs of growth rate and sliding speed.

Fourier Model for Continuous Contact

The one-dimensional Fourier finite element model serves for the validation and convergence study of the continuous contact solution. It is constructed in a way similar to the one used in Yi [13]. The model is discretized in the thickness only and each node has two degrees of freedom along the x- and y-directions. The wave number appears in both stiffness and thermal matrices in the finite element equations. The cyclic boundary conditions and coextensive contact are the intrinsic features of the model. Therefore the computational effort is minimized in the Fourier model as the finite element discretization is not needed in the direction of sliding.

Nonconductive Rigid Friction Plate

To consider the extreme situation where a conductive half plane slides against a rigid nonconductive surface in the finite element models, a sufficiently large thickness equal to the circumferential length of the disk is assumed in the conductive material so that the boundary effects are minimized. Meanwhile the elastic modulus of the insulating material is set to a value five orders of magnitude higher than that of the conductive material, and a single element is used across the thickness of the insulator. Other parameters remain unchanged.

ANALYTICAL MODELS FOR COMPARISON

Continuous Contact

Burton et al. [14] showed that for plane strain, the critical speed of a conductive surface sliding against a rigid nonconductive surface is linearly proportional to the wave number according to

$$V_c = \frac{2Km(1-\nu)}{E\alpha f} \tag{7}$$

where K is the thermal conductivity; m is the wavenumber per 2π of length; E, α, ν, f are Young's modulus, the coefficient of thermal expansion, Poisson's ratio and the coefficient of Coulomb friction, respectively.

Intermittent Contact

For a conductive half plane sliding against a rigid nonconductive surface we define the following dimensionless velocities following Ayala's notations [8]:

$$V^* = \frac{V}{km} \tag{8}$$

where V is the critical sliding velocity in the intermittent contact, and

$$V_0 = \frac{V_c}{km} \tag{9}$$

We further define a dimensionless speed $\widehat{V}$ by taking the ratio of V^* to V_0.

$$\widehat{V} = \frac{V^*}{V_0} = \frac{V}{V_c} \tag{10}$$

It was shown [8] that at sufficiently small $F_o \ll 1$,

$$\widehat{V} \to \frac{1}{R_1} \tag{11}$$

Namely, the critical speed is the same as that of a system in continuous contact with the heat generation rate replaced by the average rate during the intermittent process. Detailed numerical studies show that the critical speed differs from that predicted from Eq. (11) by less than 1% for $F_o < 0.1$.

As $F_o \to \infty$, it is found that

$$\widehat{V} \to \frac{1 + \sqrt{R_1}}{2R_1} \tag{12}$$

where R_1 is t_1/t_0, i.e., the ratio of the contact period to the overall time. For large but finite Fourier numbers, one has to solve a nonlinear equation in the following form for b^*, the dimensionless growth rate:

$$e^{(b^*R_1 - R_2)F_o} \times \left[\sqrt{1+b^*}\, e^{R_2F_o} erfc\left(\sqrt{R_2F_o}\right) - e^{(1+b^*)R_2F_o} erfc\left(\sqrt{R_2F_o(1+b^*)}\right)\right] = \frac{b^*}{1+\sqrt{1+b^*}} \tag{13}$$

from which $\widehat{V}$ can be computed from

$$b^* = \frac{1}{2}\left[4\hat{V} - 1 - \sqrt{8\hat{V}+1}\right] \tag{14}$$

Notice that "*erfc*" in Eq. (13) is the complementary error function. Equations (11) through (14) are adapted from Ayala's solutions [8].

RESULTS

A Conductive Half Plane Sliding Against a Rigid Nonconductive Surface

Continuous contact. This is a limiting case of intermittent contact with the contact ratio $R_1 = 1$. In continuous contact it is expected that the one-dimensional Fourier finite element model yields the same result as Burton's solution. In Figure 2 clearly $\widehat{V}$ of the Fourier model remains at 1.0 for the entire range of F_o. The Fourier number covered in the range corresponds to the wave number n = 1−20, or m = 6.25−125 when the disk radius r is set to 0.16 m. A convergence study for the two-dimensional finite element model is also shown in the same figure. It converges to unity at lower F_o but deviates from unity at larger F_o. We found that 24 elements in the circumference result in a maximum numerical error of approximately 20%.

In fact, when $n = 20$, each wave is covered by only one element, hence inadequate to delineate the profile of the eigenfunction at larger wave numbers. On the other hand, when the element number increases to 40 or 60, a much better accuracy is obtained. For example, with the total element number of 60, the maximum numerical error obtained is less than 1%. We conclude that the two-dimensional finite element model for continuous contact must be discretized in such a way that each wave is covered by at least two or three elements in order to achieve a desirable accuracy in the solution. In the preceding results, 12 biased elements with a bias ratio of 2.0 in the thickness direction of the conductive material have been found sufficient to capture the rapid change in the temperature gradient in the thickness.

Intermittent contact. The plane finite element model was also compared to Ayala's solution when the contact is intermittent. We did not reproduce the entire analytical solution; however, the results in the three limiting cases represented by Eqs. (11), (12), and (14) are believed to be sufficient for the purpose of comparison and validation. In the finite element model for intermittent contact, the metal layer

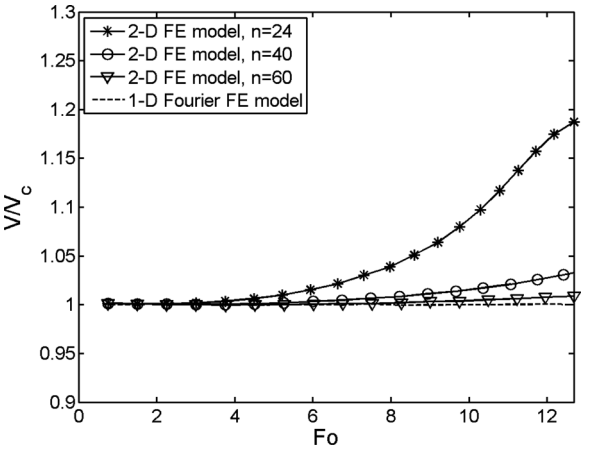

Figure 2 Convergence study of the finite element models for continuous contact, assuming a conductive half plane sliding against a rigid nonconductor.

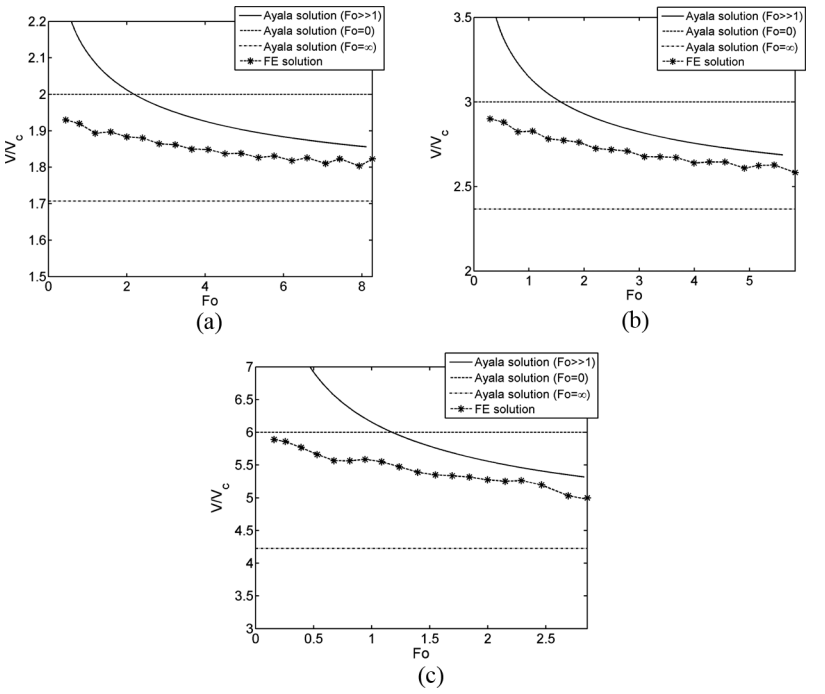

Figure 3 Finite element (FE) solutions for three different contact ratios (a) $R_1 = 1/2$, (b) $R_1 = 1/3$, and (c) $R_1 = 1/6$. A conductive half plane sliding against a rigid nonconductor is assumed.

has been divided into as many as 90 elements in the direction of sliding, so that the contact region is covered by sufficient elements. The thickness is divided into 12 elements. Figures 3(a), (b), and (c) show the finite element solutions for three different contact ratios $1/2$, $1/3$, and $1/6$, respectively.

Clearly, in all three scenarios, the results are bounded between the analytical solutions given by Eq. (11) and Eq. (12). To the right side of the figures when F_o increases, the curves gradually approach the asymptotic solutions for $F_o = \infty$. When R_1 is reduced, the figures show a reduced range of F_o, e.g., the maximum F_o is 2.8 when $R_1 = 1/6$ as opposed to 8.2 when $R_1 = 1/2$. This is because the raised critical sliding speed as a result of the reduced R_1 leads to a reduction in the total period of sliding process, and thus a decreased Fourier number.

The maximum Fourier numbers shown in Figure 3 correspond to a total wave number n of approximately 20 along the entire length of the conducting layer. Assuming 90 quadratic elements along the length, there are only about four elements for each wave. A Fourier number beyond the reported maximum value would lead to insufficient elements covered by each wave, especially at the locations where the transition between separation and contact takes place. It is believed that the range of the Fourier number in Figure 3 is adequate to show the trend of the critical speed as a function of F_o. The zigzag patterns in the curves reflect the numerical errors from the finite element analysis. These errors are actually quite small in view of the scale used for the vertical axes in the figures.

Two Conductive Plates with Finite Thickness

Continuous contact. For the continuous contact problem of two conductive, deformable plates with finite thickness, we compared the computational results between the two finite element models: (A) the full two-dimensional finite element model with both thickness and length directions discretized, and (B) the one-dimensional Fourier model defined in the thickness direction only. The parameters used in the finite element analysis are shown in Table 1. The element numbers used in the length and thickness of model A are 50 and 20, respectively. Notice that both materials are conductive now and hence both need to be divided into biased elements through the thickness. We define the dimensionless velocity in the following way:

$$\widetilde{V} = \frac{V}{V_f} \tag{15}$$

where V and V_f are the critical speeds determined by model A and B, respectively. During the calculation of V_f in the continuous contact model, the time-averaged frictional heat input (i.e., the coefficient of friction divided by R_1) is already taken into consideration. The dimensionless wave number here is defined as

$$A = ma \tag{16}$$

following Lee and Barber's notation [15].

The reason to change the definition of the dimensionless wave number is that the Fourier number F_o defined previously is no longer a monotonic function of the wave number m when the disk has a finite thickness. Figures 4(a) and (b) show the dimensionless critical speed based on Lee's notation and the definition in Eq. (15), respectively. It can be seen from Figure 4(b) that the full 2-D model agrees quite well with the Fourier model, with a maximum numerical error around 5%. The contour plots in Figure 5 display the temperature distribution with an exaggerated thickness. There is a noticeable change in the phase angle across the thermal skin layer of the poor conductor. This observation is consistent with the prior research on the subject.

Intermittent contact. Now we turn our attention to the realistic situation in which both surfaces in intermittent contact are deformable and conductive. Figure 6

Table 1 Parameters used in the intermittent contact model with both surfaces conductive and deformable

	Metal (cast iron)	Friction material
Young's modulus, E (GPa)	112.4	2.03
Poisson's ratio, v	0.25	0.35
Coefficient of thermal expansion, $\alpha\,(K^{-1})$	1.325×10^{-5}	3.0×10^{-5}
Thermal conductivity, K (W m^{-1} K^{-1})	57	0.93
Thermal diffusivity, k (mm^2 s^{-1})	17.2	0.522
Thickness (mm)	14	10
Coefficient of friction	0.4	0.4

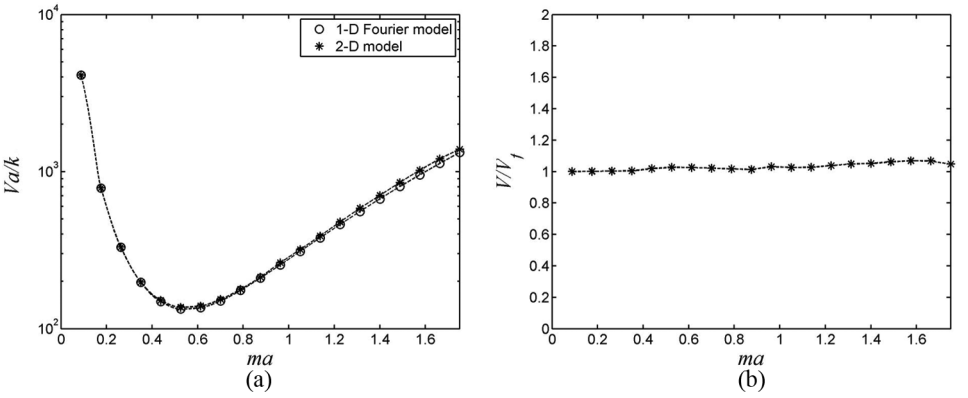

Figure 4 Dimensionless critical speed based on (a) Lee and Barber's definition [15] and (b) the definition given in Eq. (15). A conductive half plane sliding against a rigid nonconductor is assumed.

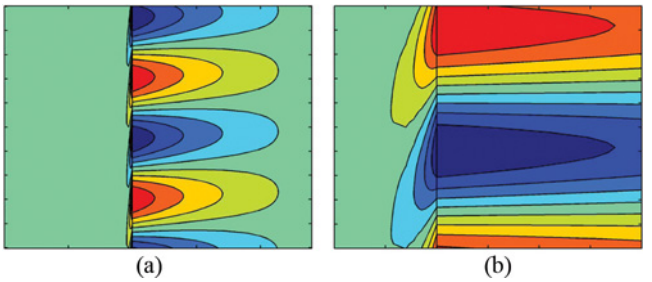

Figure 5 Temperature eigenfunction in continuous contact with the thickness exaggerated: (a) the entire model; (b) an enlarged local region on the sliding interface.

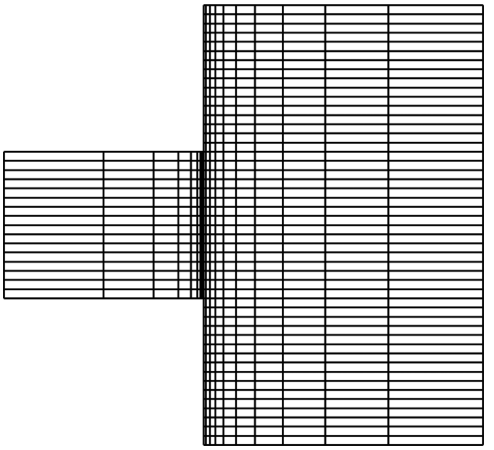

Figure 6 A biased finite element mesh generated for the model with $R_1 = 1/3$. Both sliding surfaces are conductive and deformable. The thicknesses of both layers are exaggerated.

shows an example of the finite element mesh used in the computation for $R_1 = 1/3$. The model consists of 48 elements in the sliding direction and 24 elements through the thickness. For smaller values of R_1 such as $1/6$, an element number up to 60 is used in the direction of sliding to ensure that the contact region is covered by sufficient elements. The computation is performed iteratively at 20 different sliding speeds with a uniform spacing to search for the critical values of the speed.

Figures 7(a) and (b) are the results for the intermittent contact model with both materials being conductive and deformable. Figure 7(b) indicates that the continuous contact model with the time-averaged frictional heating always overestimates the critical speed, which is consistent with the conclusion from the prior analytical studies. However, Figure 7 reveals several new features that are quite different from the half-plane solution. First of all, the dimensionless speed $\widetilde{V}$ is no longer a monotonic

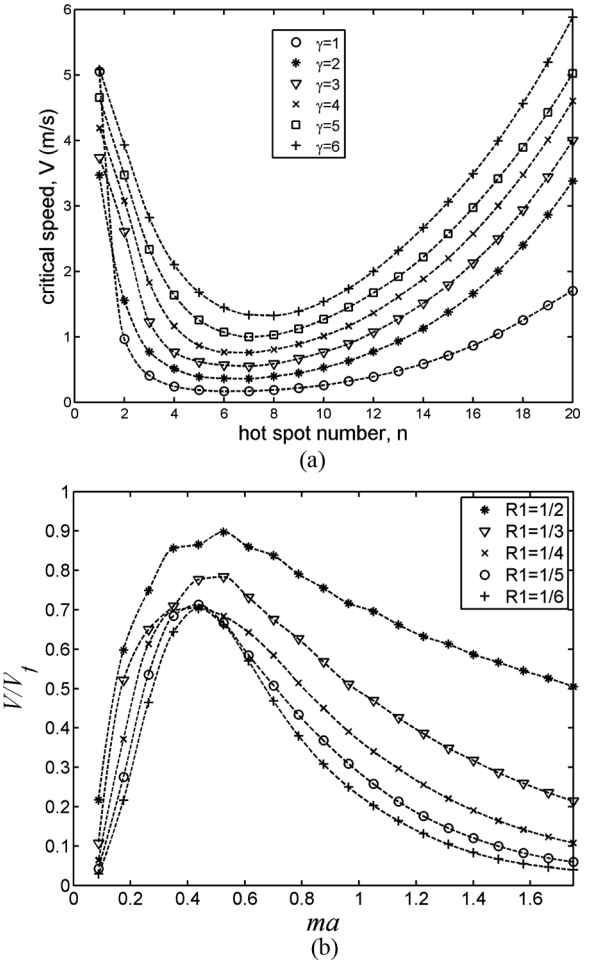

Figure 7 Critical speed in intermittent contact as a function of the wave number, where γ is the reciprocal of the contact ratio, or $1/R_1$. V_f is the critical speed in the continuous contact model, with the time-averaged frictional heat input considered.

function of the wave number. At smaller wave numbers the result is approaching zero rather than converging to Ayala's solution ($\widetilde{V} = \widehat{V}R_1 = 1$).

There exists a peak value on the curve (it is actually corresponding to the lowest value of the dimensional critical speed) where the two solutions are the closest. Particularly, when $R_1 < 1/2$, i.e., the period of contact is longer than the period of separation, applying the time-averaged heat input in the continuous contact model yields an error less than 10%. When $R_1 = 1/3$, the error becomes approximately 20%. The error is even more significant when the contact ratio is reduced further. The location of *ma* at the peak value is dependent on R_1 and it shifts slightly to the left when R_1 is reduced. Moreover, at larger wave numbers, the critical speed does not converge to Ayala's solution, either. This can be seen from a comparison between the results shown on the right side of Figure 7(b) and Eq. (12) that indicates

$$\widetilde{V} = \widehat{V}R_1 \to \frac{(1+\sqrt{R_1})}{2} \tag{17}$$

For instance, when $R_1 = 1/2$, the finite element model gives $\widetilde{V} = 0.5\text{V}$, which is much lower than Ayala's solution around 0.85. It is found that for a smaller value of R_1, the deviation of the result from Ayala's solution is even more pronounced. In fact, Ayala's solution always overestimates the critical speed, which is not surprising because of the significant difference in the fundamental assumptions related to the geometrical configurations and materials involved in the two models.

The eigenfunction of temperature shown in Figure 8(b) exhibits two distinct zones where the amplitude of oscillation either rises or decays, corresponding to the contact zone and the separation zone, respectively. Thermally, these periods are associated with the periods of frictional heating that alternate with the periods of conductive cooling. In steady state when the growth rate is zero, the

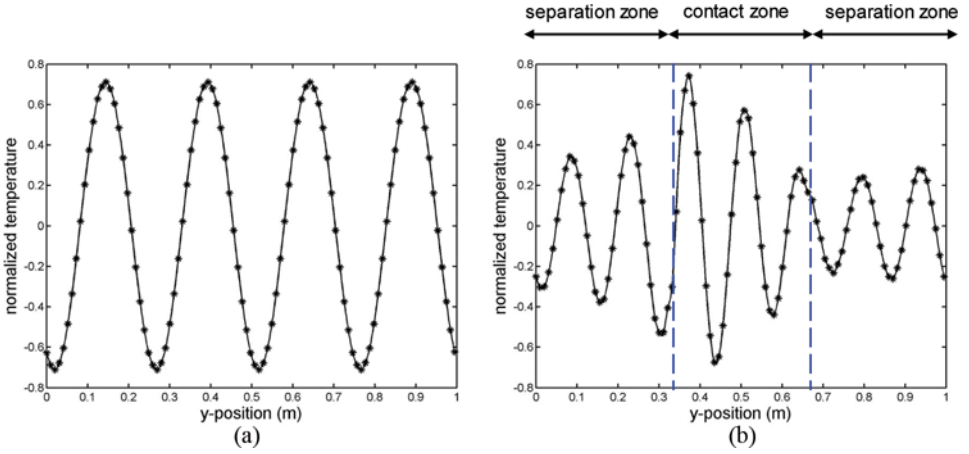

Figure 8 Representative eigenfunctions of temperature in (a) continuous contact and (b) intermittent contact with $R_1 = 1/3$.

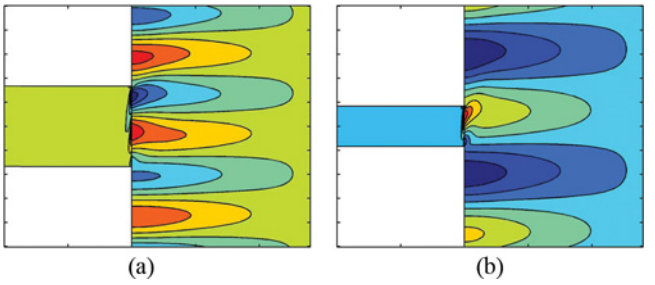

Figure 9 Eigenfunctions of temperature for intermittent contact with the contact ratio (a) $R_1 = 1/3$ and (b) $R_1 = 1/6$, presented in the form of contour plots. The thicknesses of both layers are exaggerated.

increased temperature variation due to frictional heating during the contact period is counteracted by the reduced amplitude in the separation period.

In contrast, the continuous contact model exhibits no such variations in the amplitude as seen in Figure 8(a). The temperature distribution is also presented in the contour plots in Figure 9 where the contact ratios are $R_1 = 1/3$ in (a) and $R_1 = 1/6$ in (b). It is seen that the otherwise homogeneous distribution of temperature along the contact interface becomes disturbed. A closer inspection on the eigenfunctions reveals that the temperature distribution is severely distorted near the contact/separation points where the stress concentrations are located.

CONCLUSIONS

The finite element scheme based on the eigenvalue method is implemented for the analysis of thermoelastic instability in intermittent sliding contact with practical model parameters. A numerical algorithm is developed to determine the critical velocities by tracking the eigenmode patterns and the corresponding growth rates. The method has been validated by both analytical and numerical solutions in some limiting situations. It is concluded that when the realistic materials and geometric configurations are considered for intermittent contact, neither the strategy of time-averaged heat input nor the analytical solution derived from the half-plane model works properly.

The finite element analysis reveals a bell-shaped relationship between the dimensionless critical speed and the wavelength: for longer waves the dimensionless critical speed approaches zero rather than unity; for shorter waves the critical speed is much lower than that predicted by the analytical half-plane solution. There exists a location where the dimensionless critical speed is the maximum. In general, the strategy by averaging the heat input over the entire circumference is appropriate only when the period of frictional contact is longer than the period of separation, and when the peak value of the dimensionless critical speed is our primary concern.

FUNDING

The corresponding author would like to express appreciation for the financial support provided by Beijing Institute of Technology during his sabbatical leave from the University of Denver in Fall 2013.

REFERENCES

1. J. R. Barber, Thermoelastic Instabilities in the Sliding of Conforming Solids, *Proceedings of the Royal Society of London Series A*, vol. 312, pp. 381–394, 1969.
2. L. Afferrante, M. Ciavarella, and J. R. Barber, Thermoelastodynamic Instability (TEDI): A New Mechanism for Sliding Instability, *Proceedings of the Royal Society of London Series A*, vol. 462, pp. 2161–2176, 2006.
3. P. Zagrodzki, K. B. Lam, E. Al-Bahkali, and J. R. Barber, Nonlinear Transient Behavior of a Sliding System with Frictionally Excited Thermoelastic Instability, *ASME Journal of Tribology*, vol. 123, pp. 699–708, 2001.
4. S. Du, P. Zagrodzki, J. R. Barber, and G. M. Hulbert, Finite Element Analysis of Frictionally-Excited Thermoelastic Instability, *Journal of Thermal Stresses*, vol. 20, pp. 185–201, 1997.
5. P. Zagrodzki, Thermoelastic Instability in Friction Clutches and Brakes – Transient Modal Analysis Revealing Mechanisms of Excitation of Unstable Modes, *International Journal of Solids and Structures*, vol. 46, pp. 2463–2476, 2009.
6. J. R. Barber, T. W. Beamond, J. R. Waring, and C. Pritchard, Implications of Thermoelastic Instability for the Design of Brakes, *ASME Journal of Tribology*, vol. 107, pp. 206–210, 1985.
7. D. L. Hartsock and J. W. Fash, Effect of Pad/Caliper Stiffness, Pad Thickness, and Pad Length on Thermoelastic Instability in Disk Brakes, *ASME Journal of Tribology*, vol. 122, pp. 511–518, 2000.
8. J. R. R. Ayala, K. Lee, M. Rahman, and J. R. Barber, Effect of Intermittent Contact on the Stability of Thermoelastic Sliding Contact, *ASME Journal of Tribology*, vol. 118, pp. 102–108, 1996.
9. Y. B. Yi, S. Q. Du, J. R. Barber, and J. W. Fash, Effect of Geometry on Thermoelastic Instability in Disk Brakes and Clutches, *ASME J. Tribology*, vol. 121, pp. 661–666, 1999.
10. P. Decuzzi and G. Demelio, The Effect of Material Properties on the Thermoelastic Stability of Sliding Systems, *Wear*, vol. 252, pp. 311–321, 2002.
11. Y. B. Yi, J. R. Barber, and P. Zagrodzki, Eigenvalue Solution of Thermoelastic Instability Problems Using Fourier Reduction, *Proceedings of the Royal Society of London Series A*, vol. 456, pp. 2799–2821, 2000.
12. Y. B. Yi, *Finite Element Analysis of Frictionally Excited Thermoelastic Instabilities in Automotive Brakes and Clutches*, Ph.D. Dissertation, University of Michigan, 2001.
13. Y. B. Yi, Finite Element Analysis of Thermoelastodynamic Instability Involving Frictional Heating, *ASME Journal of Tribology*, vol. 128, pp. 718–724, 2006.
14. R. A. Burton, V. Nerlikar, and S. R. Kilaparti, Thermoelastic Instability in a Seal-Like Configuration, *Wear*, vol. 24, pp. 177–188, 1973.
15. K. J. Lee and J. R. Barber, Frictionally-Excited Thermoelastic Instability in Automotive Disk Brakes, *ASME Journal of Tribology*, vol. 115, pp. 607–614, 1993.